Field-Cycling Long-Lived-State NMR of $^{15}N_2$ Spin Pairs

Stuart J. Elliott[a,*], Pavel Kadeřávek[b], Lynda J. Brown[a], Mohamed Sabba[a], Stefan Glöggler[c], Daniel J. O'Leary[d], Richard C. D. Brown[a], Fabien Ferrage[b], Malcolm H. Levitt[a]

[a] *School of Chemistry, University of Southampton, Southampton SO17 1BJ, United Kingdom*
[b] *Laboratoire des Biomolécules, Département de Chimie, UMR 7203 CNRS-UPMC-ENS, Ecole Normale Supérieure, 24 Rue Lhomond, 75231 Paris Cedex 05, France*
[c] *Max-Planck-Institute for Biophysical Chemistry, Am Fassberg 11, 37077 Göttingen, Germany*
[d] *Department of Chemistry, Pomona College, 645 North College Avenue, Claremont, California 91711, United States of America*

Abstract

A range of nuclear magnetic resonance spectroscopy and imaging applications are limited by the short lifetimes of magnetization in solution. Long-lived states, which are slowly relaxing configurations of nuclear spins, have been shown to alleviate this limitation. Long-lived states have decay lifetimes $T_{\rm LLS}$ significantly exceeding the longitudinal relaxation time T_1, in some cases by an order of magnitude. Here we present an experimental case of a long-lived state for a ^{15}N labelled molecular system in solution. We observe a strongly biexponential decay for the long-lived state, with the lifetime of the slowly relaxing component exceeding 40 minutes, ∼21 times longer than the spin-lattice relaxation time T_1. The lifetime of the long-lived state was revealed by using a dedicated two-field NMR spectrometer capable of fast sample shuttling between high and low magnetic fields, and the application of a resonant radiofrequency field at low magnetic field. The relaxation characteristics of the long-lived state are examined.

Keywords: long-lived states, $^{15}N_2$ spin pair, field-cycling, two-field NMR spectrometer

1. Introduction

Nuclear magnetic resonance spectroscopy (NMR) and imaging (MRI) are unrivalled tools for the determination of molecular structure and dynamics. However, some applications of NMR and MRI such as hyperpolarization [1–3], diffusion [4, 5] and measurements of slow processes [6, 7] would ultimately prosper from an increased time period in which nuclear spin order is preserved. Such capabilities would allow the study of dynamic processes which are relatively slow compared to the spin-lattice relaxation time T_1. Long-lived states (LLS) provide an opportunity to maintain nuclear spin order for extended times [8, 9]. For systems of spin-1/2 pairs, the long-lived state is immune to in pair dipolar relaxation, with other symmetric decay mechanisms strongly attenuated [10–18]. LLS have relaxation time constants denoted $T_{\rm LLS}$, which often transcend T_1 by a large factor. Potential applications of LLS include hyperpolarized imaging and transport [19, 20], and the study of enzymatic reactions and ligand binding [21–23].

A number of molecular structures exhibiting large $T_{\rm LLS}/T_1$ ratios have previously been demonstrated. An asymmetric *cis*-fumarate diester supports a proton long-lived state of ∼10 minutes and a $T_{\rm LLS}/T_1$ ratio of ∼50 at high field [24, 25]. A ∼77 minute long-lived state is provided by a ^{13}C labelled naphthalene derivative in room temperature solution [26], and a ^{15}N labelled diazirine spin pair exhibits a long-lived state of ∼23 minutes at low field [27]. The long-lived state of ^{15}N-nitrous oxide has been recorded utilizing field-cycling equipment and surpasses 26 minutes in solution [28].

In this paper we present a ^{15}N labelled molecular structure (Figure 1) exhibiting a long-lived state lifetime exceeding 40 minutes in solution. This system ($^{15}N_2$-**I**) is constructed by a Diels-Alder reaction of (*S*)-4-(1-phenylethyl)-3*H*-1,2,4-triazole-3,5(4*H*)-dione-1,2-$^{15}N_2$ and a fully deuterated cyclopentadiene. Although the spin-lattice and long-lived state relaxation times are relatively short at high field, impressive relaxation times are unveiled at low field. The decay of the long-lived state is biexponential, with the slowly relaxing component having a time constant ∼21 times longer than T_1. Experiments at low field make use of a dedicated two-field NMR spectrometer which allows fast transfer of a sample shuttle between two magnetic field centres operating at different magnetic fields (14.1 T and 0.33 T), and with radiofrequency irradiation at low magnetic field. The dipolar relaxation mechanisms of the long-lived state are discussed.

2. Experimental Methods

The molecular system selected for study was 2-((*S*)-1-phenylethyl)-5,8-dihydro-1*H*-5,8-methano[1,2,4]triazolo[1,2-*a*]pyridazine-1,3(2*H*)-dione-5,6,7,8,10,10-d_6-4,9-$^{15}N_2$ ($^{15}N_2$-**I**) and was prepared by

*Corresponding author
Email address: sje1g13@soton.ac.uk (Stuart J. Elliott)

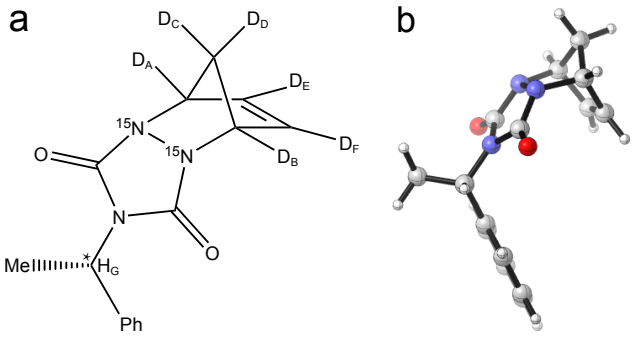

Figure 1: Molecular structure of $^{15}N_2$-**I**; (a) showing the chiral centre ($*$) which is implicated in the chemical inequivalence of the ^{15}N labelling sites, and (b) displaying the lowest energy conformer in vacuum [31]. White spheres = hydrogen atoms, grey spheres = carbon atoms, purple spheres = nitrogen nuclei, red spheres = oxygen atoms.

a rapid room temperature Diels-Alder cycloaddition of (*S*)-4-(1-phenylethyl)-3*H*-1,2,4-triazole-3,5(4*H*)-dione-1,2-$^{15}N_2$ and fully deuterated cyclopentadiene. Freshly prepared cyclopentadiene was perdeuterated (95 atom % D) by five cycles of proton-deuterium exchange using NaOD in DMSO/D_2O [29]. (*S*)-4-(1-phenylethyl)-1,2,4-triazolidine-3,5-dione-1,2-$^{15}N_2$ was synthesised from $^{15}N_2$ hydrazine and (*S*)-α-methylbenzyl isocyanate by adaptation of the procedure described by Cookson *et. al.* [30]. For further details of the synthetic route to $^{15}N_2$-**I** see the Supporting Information (SI). Sample preparation for two-field NMR experiments: 29.1 mg of $^{15}N_2$-**I** was dissolved in 106 μL of CD_2Cl_2 solvent at a concentration of 1 M. The solution was transferred to a glass shuttling tube which was sealed with glue. Samples were prepared under an argon atmosphere to displace the majority of molecular oxygen.

The relevant portion of the experimental ^{15}N NMR spectrum of $^{15}N_2$-**I** is shown in Figure 2. The characteristic AB spectral pattern of the inequivalent $^{15}N_2$ spin pair is well-resolved, and indicates a chemical shift difference which is a similar magnitude to the in pair J-coupling. The spectrum may be simulated using a J-coupling of $|J_{NN}| = 11.7 \pm 0.1$ Hz and an isotropic chemical shift difference of $\Delta\delta_{NN} = 199 \pm 3$ ppb between the labelled ^{15}N sites, corresponding to 12.1 $\pm$ 0.2 Hz at the 14.1 T magnetic field.

The small chemical shift difference is due to: (i) a chiral centre three bonds away from the $^{15}N_2$ spin pair; and (ii) an out-of-plane carbon-bridge structure which creates a conformational population bias in the rotation of the chiral group. These factors combine to generate a small chemical shift difference between the ^{15}N sites after averaging over all conformations.

The small isotropic chemical shift difference between the ^{15}N labelling sites of $^{15}N_2$-**I** is reproduced remarkably well by quantum chemistry computations [32–34]. The ^{15}N chemical shift difference was estimated to be 176 ppb after averaging over the rotation of the chiral group (Figure 1a, $*$), see the Supporting Information (SI) for details.

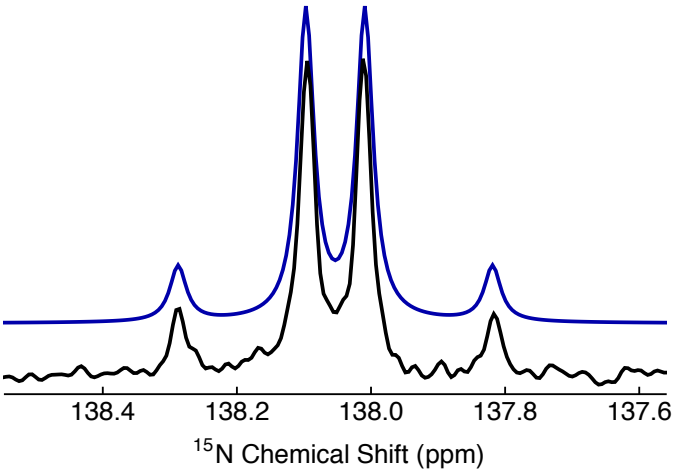

Figure 2: Relevant portion of the experimental ^{15}N NMR spectrum of 1 M $^{15}N_2$-**I** in CD_2Cl_2 solution acquired at 14.1 T (60.8 MHz) and 22 °C with a single transient. Black line: experimental ^{15}N spectrum; Blue line: simulation ($|J_{NN}| = 11.7 \pm 0.1$ Hz, $\Delta\delta_{NN} = 199 \pm 3$ ppb) using Lorentzian line broadening (half-width at half height = 1.8 Hz). The inner splitting of the black spectrum is 5.1 Hz.

The isotropic chemical shift difference allows access to the long-lived state of the ^{15}N nuclei, by using radiofrequency pulse techniques, and their variants, which operate in the near-equivalence regime [35–41]. In the current study, we used the M2S (Magnetization-to-Singlet) method [35, 36], as shown in Figure 3. The M2S pulse sequence was preferred due to its robustness. Details of the pulse sequence optimization are given elsewhere [35, 36].

After a single 90_{90} pulse converts longitudinal magnetization into transverse magnetization at high magnetic field (HF, 14.1 T), the M2S method works as follows: (1) consecutive Δ-180_{COMP}-Δ modules establish triplet-singlet coherences; (2) an individual 90_0 pulse transforms the transverse magnetization into zero-quantum triplet-singlet coherences; (3) a synchronized delay Δ π-shifts the phase of the coherences generated in (2); (4) a second Δ-180_{COMP}-Δ cycle creates a triplet-singlet population difference. 180_{COMP} specifies the following composite 180° rotation: $90_0180_{90}90_0$. The echo trains in (2) and (4) are repeated n_1 and n_2 times, respectively, and $\Delta \simeq (4J_{NN})^{-1}$, neglecting relaxation and other complications [35, 36].

NMR experiments for measuring the LLS relaxation rate of $^{15}N_2$-**I** at low magnetic field (LF, 0.33 T) were performed using a dedicated two-field NMR spectrometer [42, 43]. The sample was transported from HF to LF using a pneumatic shuttling device [44]. The rapid sample shuttling is not strictly necessary for this experiment; the rapid shuttle was used for convenience.

The long-lived state is allowed to evolve in LF for a time τ_{EV} in the presence of continuous wave (CW) irradiation at the low magnetic field ^{15}N resonance frequency of 1.4 MHz (nutation frequency = 500 Hz). As discussed in a separate paper [45], the relaxation of $^{15}N_2$ singlet order is strongly influenced by the spin-lattice relaxation of the nearby deuterons, through scalar relaxation of the second kind. This mechanism is efficiently suppressed by the

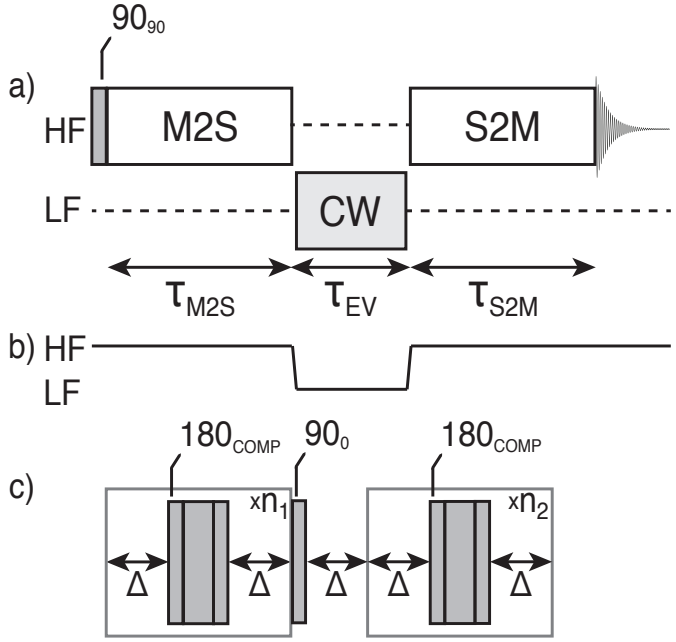

Figure 3: a) Pulse sequence used for preparing a long-lived state in $^{15}N_2$-**I** and monitoring its decay. The decay of the long-lived state is tracked by repeating the pulse sequence for different values of the evolution delay τ_{EV}. Continuous wave (CW) irradiation (nutation frequency = 500 Hz) is applied to the ^{15}N spins at low magnetic field throughout the duration of τ_{EV}. A two-step phase cycle is used to remove spurious signals generated by longitudinal magnetization accrued during the M2S sequence. An interval of 900 s was used between successive transients. b) Qualitative magnetic field profile used during field-cycling experiments. Sample shuttling from high magnetic field (HF, 14.1 T) to low magnetic field (LF, 0.33 T) takes 280 ms, and from LF to HF takes 500 ms. c) Magnetization-to-singlet (M2S) pulse sequence. The long-lived state was prepared and reconverted at HF by using the following experimental parameters: Δ = 20.0 ms, $n_1 = 2$ and $n_2 = 1$. 180_{COMP} denotes a composite 180° pulse: $90_0180_{90}90_0$. The S2M sequence is a chronologically-reversed M2S sequence.

application of resonant radiofrequency irradiation at the low-field ^{15}N resonance frequency.

The sample is subsequently returned to HF by using the pneumatic shuttle, and a chronologically-reversed M2S sequence (S2M) is applied. The induced NMR signal is detected at HF. In the current study, the parameters of the M2S pulse sequence were chosen to maximise the detected signal intensity of the long-lived state: Δ = 20.0 ms, $n_1 = 2$ and $n_2 = 1$. The maximum amplitude of the ^{15}N NMR signal, relative to that induced by a single 90° pulse, was found to be 10.5%. The theoretical performance of the M2S sequence for the experimental parameters given is 19.7%. The loss relative to the theoretical maximum of 2/3 [46] is not yet fully understood but could be associated with a breakdown of the strong-coupling regime, non-adiabatic magnetic field variation during sample shuttling, radiofrequency field imperfections and relaxation.

3. Results

A decay curve for the ^{15}N long-lived state at LF is shown in Figure 4. The experimental decay (black data points) is well fitted with a bi-exponential decay function (black solid line) using two relaxation time constants, denoted

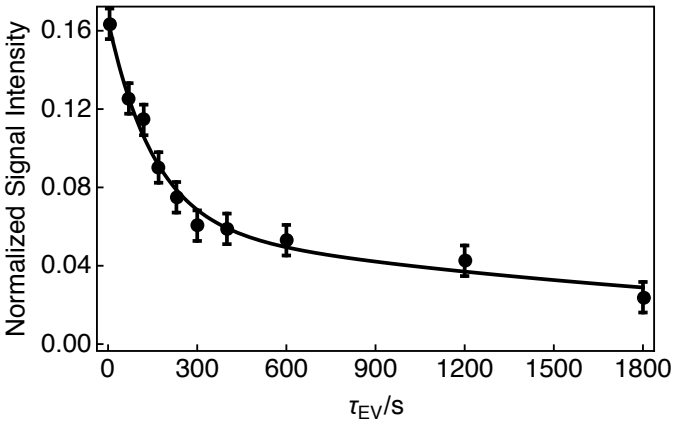

Figure 4: Experimental relaxation curve (black data points) for the long-lived state of 1 M $^{15}N_2$-**I** in CD_2Cl_2 solution acquired at 0.33 T and 22 °C with 2 transients per data point. The decay of the long-lived state was measured by using the pulse sequence described in Figure 3. All signal amplitudes were normalized to the first data point. The decay curve has a multi-exponential form, and was fitted with a bi-exponential decay function (black solid line): A exp{-t/T_A^{LF}} + B exp{-t/T_B^{LF}}. A = 0.105, $T_A^{LF} = 155 \pm 12$ s, B = 0.06, $T_B^{LF} = 2437 \pm 374$ s. Data point error bars were estimated from the standard deviation of 10 integrated noise regions outside of the $^{15}N_2$ peak area.

T_A^{LF} and T_B^{LF}. Bi-exponential decay function: A exp{-t/T_A^{LF}} + B exp{-t/T_B^{LF}}. Fit parameters: A = 0.105, $T_A^{LF} = 155 \pm 12$ s, B = 0.060, $T_B^{LF} = 2437 \pm 374$ s. We attribute the longer relaxation time constant to the decay of the long-lived state, giving $T_{LLS}^{LF} = 2437 \pm 374$ s. This is ~21 times longer than the LF relaxation time for the longitudinal magnetization of the ^{15}N sites $T_1^{LF} = 117 \pm 12$ s, as estimated from a separate inversion-recovery measurement. The time constants T_1^{LF} and T_A^{LF} (the initial portion of the LLS decay curve) are in approximate agreement.

The ^2H longitudinal relaxation times for $^{15}N_2$-**I** were measured in CD_2Cl_2 solvent at 14.1 T (107.5 MHz) and 22°C. The T_1 of the ^2H spins D_A and D_B (Figure 1a) is $T_1(^2H) = 106 \pm 6$ ms.

4. Discussion

Evaluation of the dipolar coupling contributions to the long-lived state relaxation time T_{LLS} requires an estimate of the rotational correlation time τ_C. The ^2H relaxation data allow an estimate of τ_C. The following analysis refers to data obtained on 1 M $^{15}N_2$-**I** in CD_2Cl_2 solution, at 14.1 T (107.5 MHz) and 22°C. The rotational correlation time τ_C was estimated by analysing the experimental relaxation time constant T_1^{-1} for the ^2H nuclei adjacent to the $^{15}N_2$ spin pair (Figure 1a, D_A and D_B), using equation 1 which applies for extreme-narrowing isotropic rotational tumbling [47]:

$$T_1^{-1}(^2H) = \frac{3}{2}\omega_Q^2\tau_C. \quad (1)$$

The quadrupolar coupling constant ω_Q is defined as follows:

$$\omega_Q = \frac{e^2qQ}{2\hbar}, \quad (2)$$

Table 1: Estimated dipolar coupling contributions to the LLS relaxation rate constant $T_{\rm LLS}^{-1}$(DD) for 1 M $^{15}N_2$-**I** in CD_2Cl_2 solution at 0.33 T and 22°C, assuming a rotational correlation time of τ_C = 17.8 ps. Sites are labelled as in Figure 1a. Ph = phenyl, Me = methyl, H_G = lone proton, N = ^{14}N nucleus. The LLS relaxation rate constants $T_{\rm LLS}^{-1}$(DD) from methyl and phenyl group protons have been aggregated.

Site	Isotope	r_{ik}/pm	r_{jk}/pm	θ_{ikj}/°	$T_{\rm LLS}^{-1}$(DD)/s^{-1} × 10^3
D_A	^{2}H	328.4	213.2	19.2	0.043 ± 0.002
D_B	^{2}H	213.2	328.3	19.2	0.043 ± 0.002
D_C	^{2}H	262.9	263.0	32.0	0.0167 ± 0.0009
D_D	^{2}H	334.3	334.3	25.1	0.0025 ± 0.0001
D_E	^{2}H	371.1	314.7	22.6	0.0028 ± 0.0002
D_F	^{2}H	314.7	370.9	22.6	0.0028 ± 0.0002
Ph	^{1}H				0.0053 ± 0.0003
Me	^{1}H				0.0107 ± 0.0006
H_G	^{1}H	420.8	381.1	20.1	0.0112 ± 0.0006
N	^{14}N	223.3	223.6	37.9	0.0131 ± 0.0007

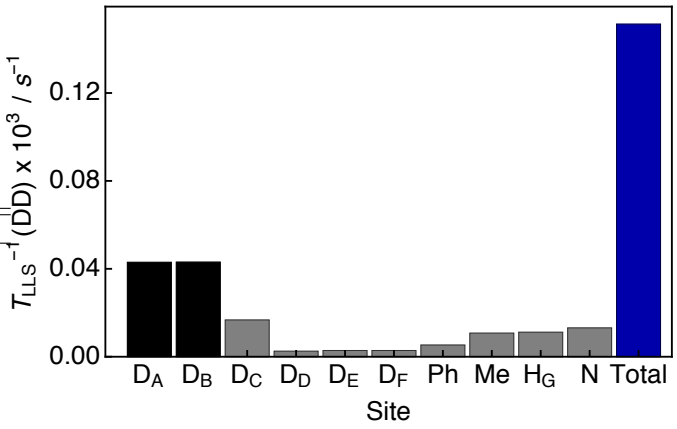

Figure 5: Theoretical intramolecular dipolar coupling contributions to the LLS relaxation rate constant $T_{\rm LLS}^{-1}$(DD) for 1 M $^{15}N_2$-**I** in CD_2Cl_2 solution at 0.33 T and 22°C, assuming a rotational correlation time of τ_C = 17.8 ps. Sites are labelled as in Figure 1a. Deuterons D_A and D_B are shown in black. Ph = phenyl, Me = methyl, H_G = CH proton, N = ^{14}N nucleus. The LLS relaxation rate constant $T_{\rm LLS}^{-1}$(DD) from methyl and phenyl group protons has been aggregated. The total LLS relaxation rate constant from intramolecular dipolar couplings is shown in blue.

where eQ is the electric quadrupolar moment of the deuterium nucleus, and eq is the electrical field gradient at the deuterium nucleus [48].

The structure of $^{15}N_2$-**I** was optimized by the quantum chemistry package *Gaussian 09* [33]. Computations employed the DFT/B3LYP/6-31G+(d,p) level of theory. The deuteron quadrupole coupling constant $\omega_Q/2\pi$ = 94.7 kHz was estimated by including the keyword "pickett" in a NMR calculation engaging the GIAO-DFT/B3LYP/6-31G(df,3p) level of theory [49]. The computations revealed two predominant rotamers for the chiral group (Figure 1a, ∗), but each possesses similar NMR parameters and only one structure (Figure 1b) is used to calculate the relaxation dynamics, see the Supporting Information (SI) for details.

From comparing the experimental relaxation time $T_1(^2\mathrm{H})$ = 106 ± 6 ms with equation 1, which was derived for the case of a molecule undergoing isotropic rotational diffusion [50], and assuming that the quadrupolar mechanism dominates the deuteron relaxation, we estimate a correlation time for the overall tumbling of the molecule in solution: τ_C = 17.8 ± 1.0 ps. The contribution of dipolar interactions to ^{2}H longitudinal relaxation is found to be negligible and is neglected.

LLS are immune to the motional modulation of the in-pair dipolar coupling, but the contribution to long-lived state relaxation from dipolar couplings originating outside the spin pair is expected to be important. Long-lived state relaxation of this kind is highly dependent on molecular geometry, and is given by [51, 52]:

$$T_{\rm LLS}^{-1}(\mathrm{DD}) = \frac{4}{3}\sum_k I_k\,(I_k+1) \times \left[\omega_{ik}^2+\omega_{jk}^2-2\omega_{ik}\omega_{jk}P_2\left(cos\left(\theta_{ikj}\right)\right)\right]\tau_C, \quad (3)$$

where the sum runs over all spins k external to the spin pair ij, θ_{ikj} is the angle subtended by the ik and jk internuclear vectors, I_k is the angular momentum quantum number of the external spin k, and $P_2(x) = (3x^2-1)/2$ is a second-rank Legendre polynomial. The dipolar coupling constant ω_{ik} is defined as follows:

$$\omega_{ik} = -\left(\mu_0/4\pi\right)\gamma_i\gamma_k\hbar r_{ik}^{-3}, \quad (4)$$

where γ_i is the magnetogyric ratio of spin i and r_{ik} is the internuclear distance between spins i and k.

The internuclear separations r_{ik},r_{jk} and subtended angles θ_{ikj} for the geometry optimized structure of $^{15}N_2$-**I** for all magnetic sites k which are external to the $^{15}N_2$ spin pair ij are shown in Table 1. The deuterons located at the base of the carbon-bridge structure (Figure 1a, D_A and D_B) are the closest to the ^{15}N spins.

Using equation 3 which applies for extreme-narrowing isotropic rotational tumbling [47], and assuming dipolar coupling constants of $\omega_{\mathrm{ND_A}}/2\pi$ = 52.8 Hz and 192.9 Hz, we obtain the following estimate of the dipolar contribution to the LLS relaxation rate constant from the deuteron D_A: $T_{\rm LLS}^{-1}(\mathrm{ND_A}) = (0.043\pm0.002)\times10^{-3}\,\mathrm{s}^{-1}$. A similar dipolar contribution is calculated for the deuteron D_B (Figure 5, black columns).

The predicted time constant for the slowly relaxing component of the biexponential decay is given by the sum of dipolar contributions within the spin system: $T_{\rm LLS}^{-1}(\mathrm{DD}) = (0.151 \pm 0.009) \times 10^{-3}\,\mathrm{s}^{-1}$ (Figure 5, blue column). The combined contribution from deuterons D_A and D_B is found to provide ∼57% of the predicted dipolar LLS relaxation rate constant for the ^{15}N spins. The combined estimate was found to be insufficient as to explain the experimental time constant: $(T_{\rm LLS}^{\rm LF})^{-1} = (0.54 \pm 0.07) \times 10^{-3}\,\mathrm{s}^{-1}$. At such long relaxation times, the discrepancy between estimated and experimental LLS decay rate constants could be attributed to a large number of relaxation mechanisms including: attenuated chemical shift anisotropy and singlet-triplet leakage [52] at LF, dipolar couplings with molecules in the solvent, and spin-rotation or spin-internal-motion

couplings [26, 53]. It is also plausible that molecular diffusion could influence the measurement of the long-lived state decay, as translation of the $^{15}N_2$ spin pair outside of the radiofrequency coil region (at long evolution delays after spin encoding) would manifest as an apparent attenuation of the nuclear singlet lifetime [40].

The biexponential nature of the LLS decay is not currently understood, but is thought to be associated with non-scalar orders which decay on the T_1 timescale and are unaffected by the change in magnetic field induced by fast sample shuttling. It is possible that the build up of such terms is related to the use of the M2S sequence. Pulsed methods to target a singlet precursor order are currently under development in our laboratories.

5. Conclusions

In summary, we have presented a ^{15}N labelled molecular system with a long-lived state exhibiting a biexponential decay. The time constant for the slowly decaying component of the biexponential decay T_{LLS} exceeds 40 minutes in solution. The ratio of T_{LLS} to T_1 was $\sim$21. The long-lived state was studied at low magnetic field by using sample shuttling apparatus housed inside a dedicated two-field NMR spectrometer. The dipolar relaxation pathways of the long-lived state were explored, and were found to be too weak to explain the experimental data. The reason for this discrepancy is not currently understood. These results are encouraging for the future construction of core molecular units which may support long-lived states, and demonstrate that $^{15}N_2$ systems house a suitable target spin pair. We are currently investigating other molecular candidates of this kind in our laboratories.

Acknowledgements

This research was supported by the Engineering and Physical Sciences Research Council (EPSRC) UK, grant codes EP/N002482 and EP/L505067/1, the European Research Council (ERC) under the European Communities Seventh Framework Programme (FP7/2007-2013), ERC Grant agreement 279519 (2F4BIODYN) (to F.F.), the Wolfson Foundation, COST STSM Action CA15209 and Bruker BioSpin UK. The authors thank Giuseppe Pileio, Pär Håkansson, Gabriele Stevanato, Aqeel A. Hussien and O. Maduka Ogba for discussions, and Sina Marhabaie for experimental help.

References

[1] P. R. Vasos, A. Comment, R. Sarkar, P. Ahuja, S. Jannin, J.-P. Ansermet, J. A. Konter, P. Hautle, B. van den Brandt and G. Bodenhausen, *Proc. Natl. Acad. Sci. U.S.A.*, 2009, **106**, 18469–18473.

[2] M. C. D. Tayler, I. Marco-Rius, M. I. Kettunen, K. M. Brindle, M. H. Levitt and G. Pileio, *J. Am. Chem. Soc.*, 2012, **134**, 7668–7671.

[3] S. J. Elliott, B. Meier, B. Vuichoud, G. Stevanato, L. J. Brown, J. Alonso-Valdesueiro, L. Emsley, S. Jannin and M. H. Levitt, *Phys. Chem. Chem. Phys.*, 2018, **20**, 9755–9759.

[4] G. Pileio and S. Ostrowska, *J. Magn. Reson.*, 2017, **285**, 1–7.

[5] M. C. Tourell, I.-A. Pop, L. J. Brown, R. C. D. Brown and G. Pileio, *Phys. Chem. Chem. Phys.*, 2018, –.

[6] S. Cavadini, J. Dittmer, S. Antonijevic and G. Bodenhausen, *J. Am. Chem. Soc.*, 2005, **127**, 15744–15748.

[7] R. Sarkar, P. R. Vasos and G. Bodenhausen, *J. Am. Chem. Soc.*, 2007, **129**, 328–334.

[8] M. Carravetta, O. G. Johannessen and M. H. Levitt, *Phys. Rev. Lett.*, 2004, **92**, 153003.

[9] M. Carravetta and M. H. Levitt, *J. Am. Chem. Soc.*, 2004, **126**, 6228–6229.

[10] R. Sarkar, P. Ahuja, D. Moskau, P. R. Vasos and G. Bodenhausen, *Chem. Phys. Chem.*, 2007, **8**, 2652–2656.

[11] W. S. Warren, E. Jenista, R. T. Branca and X. Chen, *Science*, 2009, **323**, 1711–1714.

[12] Y. Feng, R. M. Davis and W. S. Warren, *Nat. Phys.*, 2012, **8**, 831–837.

[13] Y. Feng, T. Theis, X. Liang, Q. Wang, P. Zhou and W. S. Warren, *J. Am. Chem. Soc.*, 2013, **135**, 9632–9635.

[14] K. Claytor, T. Theis, Y. Feng, J. Yu, D. Gooden and W. S. Warren, *J. Am. Chem. Soc.*, 2014, **136**, 15118–15121.

[15] Y. Zhang, P. C. Soon, A. Jerschow and J. W. Canary, *Angew. Chem. Int. Ed.*, 2014, **53**, 3396–3399.

[16] S. J. Elliott, L. J. Brown, J.-N. Dumez and M. H. Levitt, *Phys. Chem. Chem. Phys.*, 2016, **18**, 17965–17972.

[17] S. J. Elliott, L. J. Brown, J.-N. Dumez and M. H. Levitt, *J. Magn. Reson.*, 2016, **272**, 87–90.

[18] S. Gloggler, S. J. Elliott, G. Stevanato, R. C. D. Brown and M. H. Levitt, *RSC Adv.*, 2017, **7**, 34574–34578.

[19] J.-H. Ardenkjær-Larsen, B. Fridlund, A. Gram, G. Hansson, L. Hansson, M. H. Lerche, R. Servin, M. Thaning and K. Golman, *Proc. Natl. Acad. Sci. U.S.A.*, 2003, **100**, 10158–10163.

[20] G. Pileio, S. Bowen, C. Laustsen, M. C. D. Tayler, J. T. Hill-Cousins, L. J. Brown, R. C. D. Brown, J.-H. Ardenkjaer-Larsen and M. H. Levitt, *J. Am. Chem. Soc.*, 2013, **135**, 5084–5088.

[21] N. Salvi, R. Buratto, A. Bornet, S. Ulzega, I. Rentero Rebollo, A. Angelini, C. Heinis and G. Bodenhausen, *J. Am. Chem. Soc.*, 2012, **134**, 11076–11079.

[22] R. Buratto, A. Bornet, J. Milani, D. Mammoli, B. Vuichoud, N. Salvi, M. Singh, A. Laguerre, S. Passemard, S. Gerber-Lemaire, S. Jannin and G. Bodenhausen, *Chem. Med. Chem.*, 2014, **9**, 2509–2515.

[23] A. Bornet, X. Ji, D. Mammoli, B. Vuichoud, J. Milani, G. Bodenhausen and S. Jannin, *Chem. – A Eur. J.*, 2014, **20**, 17113–17118.

[24] J.-N. Dumez, J. T. Hill-Cousins, R. C. Brown and G. Pileio, *J. Magn. Reson.*, 2014, **246**, 27–30.

[25] G. Pileio, J.-N. Dumez, I.-A. Pop, J. T. Hill-Cousins and R. C. Brown, *J. Magn. Reson.*, 2015, **252**, 130–134.

[26] G. Stevanato, J. T. Hill-Cousins, P. Håkansson, S. S. Roy, L. J. Brown, R. C. D. Brown, G. Pileio and M. H. Levitt, *Angew. Chem. Int. Ed.*, 2015, **54**, 3740–3743.

[27] T. Theis, G. X. Ortiz, A. W. J. Logan, K. E. Claytor, Y. Feng, W. P. Huhn, V. Blum, S. J. Malcolmson, E. Y. Chekmenev, Q. Wang and W. S. Warren, *Sci. Adv.*, 2016, **2**, 1501438.

[28] G. Pileio, M. Carravetta, E. Hughes and M. H. Levitt, *J. Am. Chem. Soc.*, 2008, **130**, 12582–12583.

[29] J. B. Lambert and R. B. Finzel, *J. Am. Chem. Soc.*, 1983, **105**, 1954–1958.

[30] R. C. Cookson, S. S. Gupte, I. D. R. Stevens and C. T. Watts, *Org. Synth. Coll.*, 1971, **51**, 121.

[31] C. Y. Legault, *CYLview 1.0b*, Université de Sherbrooke, 2009 (http://www.cylview.org).

[32] F. Jensen, *J. Chem. Theory. Comput.*, 2008, **4**, 719–727.

[33] M. J. Frisch, G. W. Trucks, H. B. Schlegel, G. E. Scuseria, M. A. Robb, J. R. Cheeseman, G. Scalmani, V. Barone, B. Mennucci, G. A. Petersson, H. Nakatsuji, M. Caricato, X. Li, H. P. Hratchian, A. F. Izmaylov, J. Bloino, G. Zheng,

J. L. Sonnenberg, M. Hada, M. Ehara, K. Toyota, R. Fukuda, J. Hasegawa, M. Ishida, T. Nakajima, Y. Honda, O. Kitao, H. Nakai, T. Vreven, J. A. Montgomery, J. E. Peralta, F. Ogliaro, M. Bearpark, J. J. Heyd, E. Brothers, K. N. Kudin, V. N. Staroverov, R. Kobayashi, J. Normand, K. Raghavachari, A. Rendell, J. C. Burant, S. S. Iyengar, J. Tomasi, M. Cossi, N. Rega, J. M. Millam, M. Klene, J. E. Knox, J. B. Cross, V. Bakken, C. Adamo, J. Jaramillo, R. Gomperts, R. E. Stratmann, O. Yazyev, A. J. Austin, R. Cammi, C. Pomelli, J. W. Ochterski, R. L. Martin, K. Morokuma, V. G. Zakrzewski, G. A. Voth, P. Salvador, J. J. Dannenberg, S. Dapprich, A. D. Daniels, Farkas, J. B. Foresman, J. V. Ortiz, J. Cioslowski and D. J. Fox, *Gaussian 09, Revision B.01*, Wallingford CT, 2009.

[34] L. B. Krivdin, *Prog. Nucl. Magn. Reson. Spectrosc.*, 2017, **102-103**, 98–119.

[35] G. Pileio, M. Carravetta and M. H. Levitt, *Proc. Natl. Acad. Sci. U.S.A.*, 2010, **107**, 17135–17139.

[36] M. C. D. Tayler and M. H. Levitt, *Phys. Chem. Chem. Phys.*, 2011, **13**, 5556–5560.

[37] S. J. DeVience, R. L. Walsworth and M. S. Rosen, *Phys. Rev. Lett.*, 2013, **111**, 173002.

[38] T. Theis, Y. Feng, T. Wu and W. S. Warren, *J. Chem. Phys.*, 2014, **140**, 014201.

[39] A. N. Pravdivtsev, A. S. Kiryutin, A. V. Yurkovskaya, H.-M. Vieth and K. L. Ivanov, *J. Magn. Reson.*, 2016, **273**, 56–64.

[40] B. Kharkov, X. Duan, J. Canary and A. Jerschow, *J. Magn. Reson.*, 2017, **284**, 1–7.

[41] B. A. Rodin, A. S. Kiryutin, A. V. Yurkovskaya, K. L. Ivanov, S. Yamamoto, K. Sato and T. Takui, *J. Magn. Reson.*, 2018, **291**, 14–22.

[42] S. F. Cousin, C. Charlier, P. Kaderavek, T. Marquardsen, J.-M. Tyburn, P.-A. Bovier, S. Ulzega, T. Speck, D. Wilhelm, F. Engelke, W. Maas, D. Sakellariou, G. Bodenhausen, P. Pelupessy and F. Ferrage, *Phys. Chem. Chem. Phys.*, 2016, **18**, 33187–33194.

[43] S. F. Cousin, P. Kadeřávek, B. Haddou, C. Charlier, T. Marquardsen, J. Tyburn, P. Bovier, F. Engelke, W. Maas, G. Bodenhausen, P. Pelupessy and F. Ferrage, *Angew. Chem. Int. Ed.*, 2016, **55**, 9886–9889.

[44] C. Charlier, S. N. Khan, T. Marquardsen, P. Pelupessy, V. Reiss, D. Sakellariou, G. Bodenhausen, F. Engelke and F. Ferrage, *J. Am. Chem. Soc.*, 2013, **135**, 18665–18672.

[45] S. J. Elliott, C. Bengs, L. J. Brown, J. T. Hill-Cousins, D. J. O'Leary, G. Pileio and M. H. Levitt, *In Preparation*, 2018.

[46] M. H. Levitt, *J. Magn. Reson.*, 2016, **262**, 91–99.

[47] J. Kowalewski and L. Mäler, *Nuclear Spin Relaxation in Liquids: Theory, Experiments, and Applications*, CRC Press, Boca Raton, 2006.

[48] A. Jerschow, *Prog. Nucl. Magn. Reson. Spectrosc.*, 2005, **46**, 63–78.

[49] W. C. Bailey, *J. Mol. Spectrosc.*, 1998, **190**, 318–323.

[50] A. Abragam, *Principles of Nuclear Magnetism*, Clarendon Press, Oxford, 1961.

[51] M. C. D. Tayler, S. Marie, A. Ganesan and M. H. Levitt, *J. Am. Chem. Soc.*, 2010, **132**, 8225–8227.

[52] G. Pileio, J. T. Hill-Cousins, S. Mitchell, I. Kuprov, L. J. Brown, R. C. D. Brown and M. H. Levitt, *J. Am. Chem. Soc.*, 2012, **134**, 17494–17497.

[53] P. Håkansson, *Phys. Chem. Chem. Phys.*, 2017, **19**, 10237–10254.